ANNALS OF GEOPHYSICS, 68, 3, NS340, 2025; doi:10.4401/ag-9236
OPEN ACCESS

Probabilistic soil model for seismic risk assessment based on SDMT results

Ana Maria Zapata-Franco[*,1], Yeudy Felipe Vargas-Alzate[1], Dani Tarragó[1], Antonio Gens[1]

(1) Universitat Politècnica de Catalunya, Department of Civil and Environmental Engineering, Barcelona, Spain

Article history: received December 27, 2024; accepted January 7, 2025

Abstract

A geotechnical site investigation has been conducted in the southern breakwater basin of the Port of Barcelona, for which hundreds of in-situ and lab tests have been performed. Among these tests, this study focuses on the evaluation of triple points. That is, at the prospected locations, there are results from seismic dilatometer Marchetti test (SDMT), cone penetration tests (CPTu), and laboratory tests based on soil samples. By using this information, the probabilistic distribution of the dynamic and geometrical properties of the soil profiles can be properly characterized. In this way, eleven closely spaced boreholes have been used to characterise the statistical properties of the input variables. Then, it has been performed a probabilistic generation of one-thousand soil profiles, which are statistically compatible with the data provided by the eleven aforementioned boreholes. Then, it has been analysed how the elastic properties of the generated soil profiles evolve once seismic waves have passed through them. To do so, a large set of ground motion recorded in hard soils have been employed. The main objective has been to obtain mathematical arrangements exhibiting high-efficiency to predict parameters that can be used to characterize the nonlinear dynamic response of the soil. This has been achieved by employing bivariate and multivariate analyses in the log-log space. Results show that the soil response can be properly parametrized if considering intensity measures extracted from the ground motions acting at the bedrock level and specific soil parameters. Finally, fragility curves and surfaces have been derived for risk assessment purposes.

Keywords: Seismic dilatometer Marchetti test (SDMT); Probabilistic soil profiles; Dynamic soil properties; Equivalent linear method; Seismic risk assessment

1. Introduction

The dynamic response of the soil in front of seismic actions is a complex nonlinear phenomenon involving several random variables (Pitilakis and Petridis, 2022). This complexity stems from the type of rupture, proximity to the epicenter and depth, site conditions and the mechanical properties of the media through which seismic waves pass. In addition, depending on the depth, these waves modify the mechanical properties of the soil at very low shear strains (Okur and Ansal, 2007); the deeper, the lesser this variation. Consequently, a proper modelling of the seismic response of near-surface soils must therefore considers the randomness of the implied variables and the non-linearities.

Understanding the dynamic response of the soil beneath a civil structure is crucial for seismic risk studies. It is because this segment acts as an ultimate filter that amplifies or de-amplifies harmonics depending on its dynamic properties (Cruz and Miranda, 2021). Moreover, due to the importance (and sometimes because of the complexity) of the civil structures, it is necessary to analyse their seismic interaction with the soil beneath using advanced nonlinear models. In this respect, nonlinear dynamic analysis considering 3D FEM-based representations, offer valuable insights into this problem (Vargas-Alzate et al., 2024; Zapata-Franco et al., 2025). However, for computational efficiency, simplified 1D models like Kelvin-Voigt solids, which effectively approximate the dynamic response of the soil, are often used (Hardin and Scott, 1967).

In this research, data from an extensive marine geotechnical investigation have been used to characterize the soft soils of the Port of Barcelona delta. The scope included 132 continuous rotary boreholes, 168 Cone Penetration Tests (CPTU) with pore pressure measurements, 11 seismic dilatometer Marchetti test (SDMT), and a comprehensive laboratory testing program. Additionally, 11 triple-point locations have been selected for integrated tests to minimize soil disturbance (CPTu, SDMT and Borehole). This research uses data from this geotechnical investigation to characterize 11 soil profiles that can be used to quantify the statistical variability of the main properties affecting the dynamic response of the site. From these data, 1000 soil profiles statistically compatible with those derived from the geotechnical characterisation carried out in the Port have been simulated. To do so, it has been employed a computational framework originally intended to assess seismic risk in civil infrastructures (Zapata-Franco et al., 2023). It allows to consider the randomness related to the seismic hazard and the mechanical properties of both soil and civil structures. However, the main focus of this research has been to study the causal relationship between the main features of the ground motions, in terms of intensity measures (IMs), and engineering demand parameters of the soil (EDPs). Several implementations, mainly concerning random generation and degradation of soil profiles, have been performed to enhance the original computational framework developed in (Zapata-Franco et al., 2023); these implementations allow considering: i) diverse geological conditions; ii) variation in the type of materials; iii) non-uniform distribution of materials with depth; and iv) the pairing between number of records and soil profiles should not be biunivocal. These improvements allow for a more comprehensive exploration of the relationship between IMs and EDPs. Hence, the seismic risk of special facilities located in the Port can be adequately characterised.

Once the soil profiles have been generated, they have been randomly paired with a set of ground motion records, extracted from the European Seismic Database (Luzi et al., 2016), whose magnitude range between 4 and 6 Mw. This range has been selected based on the (Coburn and Spence, 2002) study, which indicates that a magnitude of around 5.5 Mw can occur in non-tectonic processes, i.e. anywhere in the world. Afterwards, for each soil profile and assigned ground motion record, a linear equivalent analysis has been performed. Based on these results, the causal relationship between the input (Seismic hazard) and output (Nonlinear soil response) has been analysed. At a first stage, IMs have been represented by scalar parameters containing information on the ground motion records (Baker, 2007). In this manner, the bivariate distributions between these scalar-based IMs and several EDPs have been employed to quantify efficiency. In this context, the latter can be defined as the ability of one variable to predict another variable (Farlie, 1960). To do so, linear and nonlinear regression analyses in the log-log space, oriented to estimate the coefficient of determination, R^2, have been performed. From the most correlated IM-EDP pairs, fragility functions have been derived. Then, enhanced vector-valued IMs ($\vec{V}$IMs), in terms of power functions, have been created. The components of these $\vec{V}$IMs can be any scalar IM together with a set of soil properties. The objective is to develop better proxies for EDPs than the ones obtained by scalar-based IMs. In this case, multi-linear and multi-nonlinear regression analyses in the log-log space, oriented to estimate the coefficient of determination, R^2, have been performed. Research on the development of vector-valued IMs can be found in (Bojórquez et al., 2012; Yakhchalian et al., 2015; Zengin and Abrahamson, 2020; Zhou et al., 2017). In fact, based on the concept of vector-valued IMs, several researchers have proposed mathematical arrangements that improve the efficiency for predicting EDPs in buildings (Fajfar et al., 1990; Pinzón et al., 2020; Reed and Kassawara, 1990). These arrangements extract information not only from scalar IMs but also from other ground motion properties (e.g. the significant duration). It has been shown that the statistical distributions derived from these enhanced equations are more correlated with the EDPs than those from scalar components. This justifies the use of other variables that can hardly be related to intensity when creating better predictors for EDPs. From the multivariate analysis, fragility surfaces have been derived, which provides a detailed representation of soil damage compared to traditional fragility curves.

According to the above, the ultimate objective of this paper has been focused on obtaining mathematical arrangements exhibiting high-efficiency to explain EDPs that can be used to characterize the nonlinear dynamic

response of soils. To perform the aforementioned calculations, energy-based and spectral IMs as well as those obtained from specific calculations of the ground motion record have been considered in the analysis.

2. Probabilistic soil model

A probabilistic soil model is used in geotechnical applications to consider the spatial (Vanmarcke, 1977) and temporal (Carrière et al., 2018) variability of soil properties. The objective is to measure how these uncertainties influence the dynamic response of civil structures. The randomness of soil properties (e.g. stiffness and damping ratio) are simulated using statistics methods and laboratory tests. As commented above, this paper adopts the computational framework presented in Zapata-Franco et al., 2023, which allows for:

a) Random generation of the dynamic features of the modelled soil profile (G_i, ρ_i, ξ_i and h_i stand for stiffness degradation, density, damping ratio and layer thickness, respectively).
b) Introduce a ground motion record at the bedrock level of a probabilistically simulated soil profile.
c) Estimate the stiffness degradation and increase of damping ratio of each soil layer based on the equivalent linear method.
d) Calculate the resulting ground motion at the surface, after propagating through the soil profile, considering the degradation of soil properties.
e) The resulting ground motion estimated in the previous step could act at the base of a civil infrastructure (building, bridge, slope, etc).

A schematic representation of these steps can be seen in Fig. 1. It is worth mentioning that this study does not consider the generation of infrastructures (Step e). Instead, the main objective is to investigate the causal relationship between IMs and EDPs; recall, the latter are extracted from the dynamic response of the soil profile.

As commented above, in order to improve the consistency of the simulated soil profiles with the real condition, several improvements have been made to the original computational framework. In particular, the standard deviation, which represents the level of variability of soil properties, has been incorporated as a depth-dependent parameter. Moreover, the interaction of different types of materials can be considered within the soil profile,

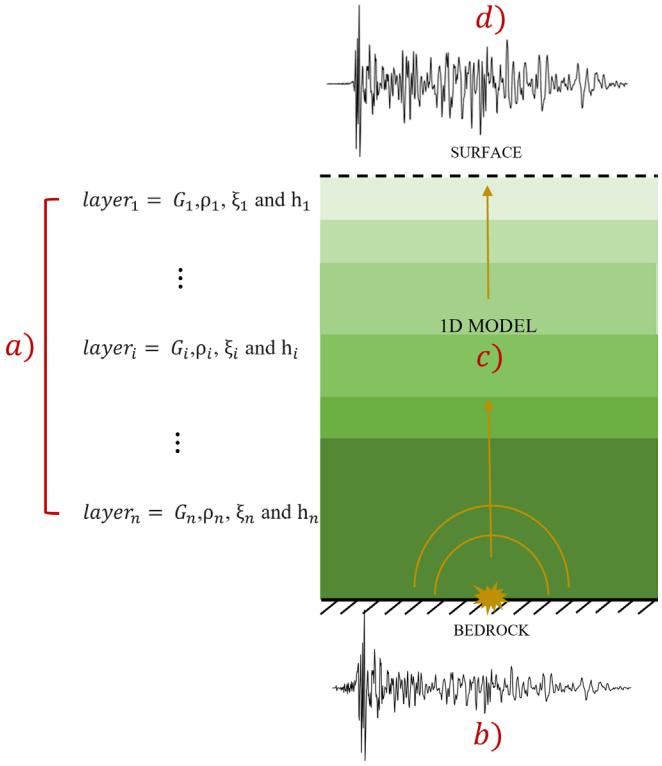

Figure 1. Computational framework diagram.

recognising its high heterogeneity. This also allows to consider the distribution of materials as a function of depth, providing an accurate representation of the evolution of material properties.

Another notable improvement relies on the restriction of having the same number of seismic signals and soil profiles. This adjustment significantly improves the practicality and usefulness of the computational framework, enabling its employment in situations where finding seismic signals is difficult or impractical. This increased adaptability makes it a versatile tool for comprehensive risk assessments in a variety of geological contexts.

2.1 Case of study

2.1.1 On-site and laboratory tests

Increasingly, there is a need to perform seismic response analyses of foundation soils, for which the shear wave velocity, Vs, serves as a fundamental input parameter. Several seismic codes and regulations (e.g. API, 2014; BSSC, 2021) recommend determining Vs at least within the first 30 meters of depth for construction projects located in seismic zones. However, this parameter has been questioned as to its reliability in quantifying soft soil effects (Castellaro et al., 2008). A more adequate quantification of site effects should take into account non-linearities and deeper soil profiles depending on the location of the bedrock.

In order to characterise the 11 basic soil profiles, the Vs obtained by SDMT tests coinciding with the triple point locations and the basic soil identification based on laboratory tests, which include granulometry, natural humidity, relative density, liquid and plastic limit, have been used to better characterise the dynamic properties of the soil in the studied area.

The SDMT is an evolution of the flat dilatometer Marchetti test (DMT) developed by S. Marchetti, 1980. In the SDMT, seismic sensors are incorporated to measure shear wave velocities (Marchetti, 2018). Moreover, this test counts with two receivers located at a distance of 0.5 meters. Thus, when a shear wave is generated from the source (Fig. 2), it reaches the upper receiver first (blue) and, after a delay, the lower receiver (red). In this manner, Vs is obtained as the difference in distance between the source and the two receivers (S2-S1), divided by the delay, Δt, in the arrival waves. The seismograms generated by the two receivers, once amplified and digitized based on depth, allow for the determination of Δt (see Fig. 2) (Marchetti et al., 2013).

On the one hand, the SDMT allows for the determination of the maximum stiffness, G_0, at small strains. On the other hand, stiffness under service conditions can be represented by the modulus of deformation (MDMT). These two stiffness values can guide the selection of degradation curves G-γ, which describe the reduction in stiffness degradation, G, as a function of shear strain, γ. Amoroso, Lehane, et al., 2012 present this methodology and define ranges where it is possible to intersect the measured data of G_0 and MDMT with previously available degradation curves. Additionally, using Vs values for clean sands, it can be estimated the potential for cyclic liquefaction by evaluating the cyclic resistance ratio (CRR) using appropriate curves (Andrus and Stokoe, 2000).

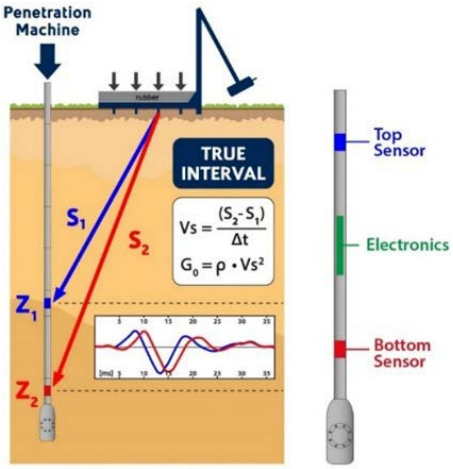

Figure 2. Diagram of SDMT, Marchetti (2018).

2.1.2 Characterization of soil profiles

Based on the geotechnical tests described in the previous section, a compilation of 11 Vs soil profiles with different stratigraphy and depths (ranging from 37 m to 40.5 m) has been developed. From the laboratory data and in-situ tests, three main groups of materials have been identified that are characteristic of continental shelf soils. In the upper strata, there has been detected a large presence of silty sands with some intrusions of organic material, whose thicknesses vary between 0.5 m and 2 m. The intermediate layers are mainly composed of silty clays (between 4 m and 15 m). In the lower layers, clayey material with some intrusions of organic soil is the most frequent configuration (between 15 m and 25 m). A summary of the thicknesses and geotechnical properties of the 11 soil profiles is given in Appendix A. This structural heterogeneity of the soil has been considered in the statistical generation of Vs profiles. Figure 3a depicts the 11 Vs soil profiles. The first and second statistical moments derived from these profiles have been used in the probabilistic simulations. In addition, Fig. 3b presents a map with the location of the 11 soil profiles, providing insight into their spatial distribution and the distances among them. This information supports the representativeness of the profiles within the study area.

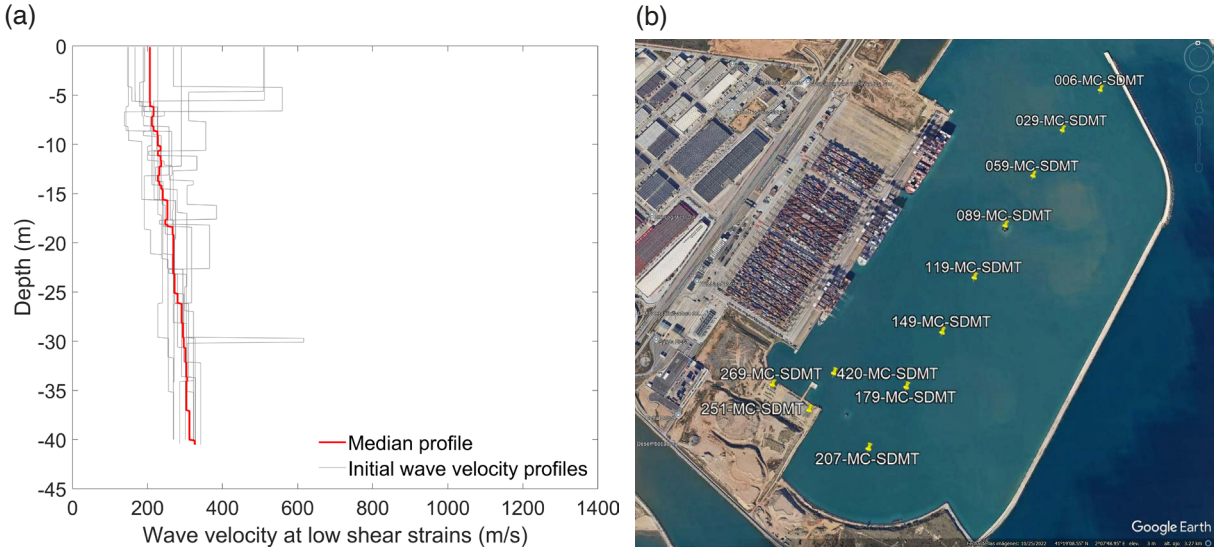

Figure 3. Soil profiles obtained from the geotechnical exploration. (a) Vs profiles. (b) Location of the geotechnical exploration.

2.2 Probabilistic generation of soil profiles

The probabilistic framework of this research considers the Toro's model to generate random soil profiles (Silva et al., 1996). This model incorporates three main elements: i) information describing the random stratigraphy at the site; ii) the median wave velocity profile; iii) the dispersion of the Vs with depth and the correlation between consecutive layers.

2.2.1 Random stratigraphy at the site

The results of the geotechnical prospections carried out in the Port of Barcelona have been used to characterize, in a probabilistic manner, the stratigraphy at the site. The "Layering Model" has been employed (Silva et al., 1996), which allows to consider that as the layer locates deeper, it becomes thicker. Hence, for each layer and respective depth of the test-based soil profiles, a cloud of transition points has been statistically parametrized; in doing so, the following power law has been adopted:

$$\lambda(h) = C_3[h + C_1]^{-C_2} \quad (1)$$

where λ is the layer boundary rate (i.e. the inverse of the thickness of the layer, 1/m) and *h* represents the depth at the middle point of the layer in meters. The estimation of the values C1, C2 and C3 has been carried out by using the capabilities of the Monte Carlo method to minimize multi-dimensional functions (Kroese and Rubinstein, 2012); Figure 4 shows this statistical parametrization. Starting from the regression line, and by considering the residuals of the dataset, the geometrical random features of the stratigraphy have been considered in the generated soil profiles.

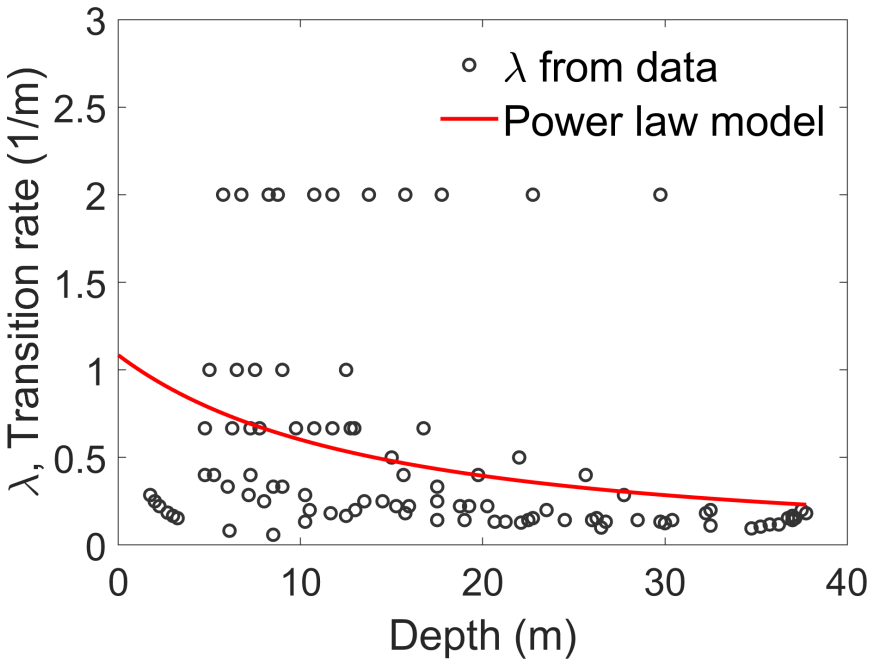

Figure 4. Relationship between the transition rate and depth.

2.2.2 The median wave velocity profile at the site

The median velocity profile shown in Fig. 3 depicts the variability with depth of the first statistical moment of the parametric distribution representing the soil profiles. Due to the cumulative character of the process associated with marine deposits, it has been observed that a log-normal distribution parametrizes adequately the aleatory character of shear wave velocities (Toro, 2022). This distribution has been adopted in the sampling process of this variable.

2.2.3 Deviations of the velocity in each layer and correlation between consecutives layers

From the test-based profiles, it has been quantified how the standard deviation evolves with depth; it can be observed that the scattering tends to decrease with depth. This feature has been incorporated in the random generation of profiles. Another important aspect observed in soil profiles is related to the spatial correlation between closer layers. The closer the layers the higher the correlation (Angelini and Heuvelink, 2018). This implies that widely separated layers tend to be less correlated. In order to consider this statistical feature, it has been assumed that the correlation between layers decreases with distance by imposing the following restrictions:

$$\rho_{i,j} = \begin{cases} i = j & \rho_{i,j} = 1 \\ i = j \pm k & \rho_{i,j} = 1 - \frac{k}{r} \geq 0 \end{cases} \tag{2}$$

where k is a number related to the position of a layer belonging to the same profile; *r* is a coefficient associated to the rate of correlation between adjacent layers. In this research, *r* has been fixed to 100/3.

2.3 Probabilistic simulation of soil profiles

Based on the aforementioned statistical features, one-thousand statistic realizations of soil profiles have been achieved via Monte Carlo simulation (Kroese and Rubinstein, 2012). The full set of Vs soil profiles can be seen in Fig. 5. It is worth to recall that they correspond to low shear strains.

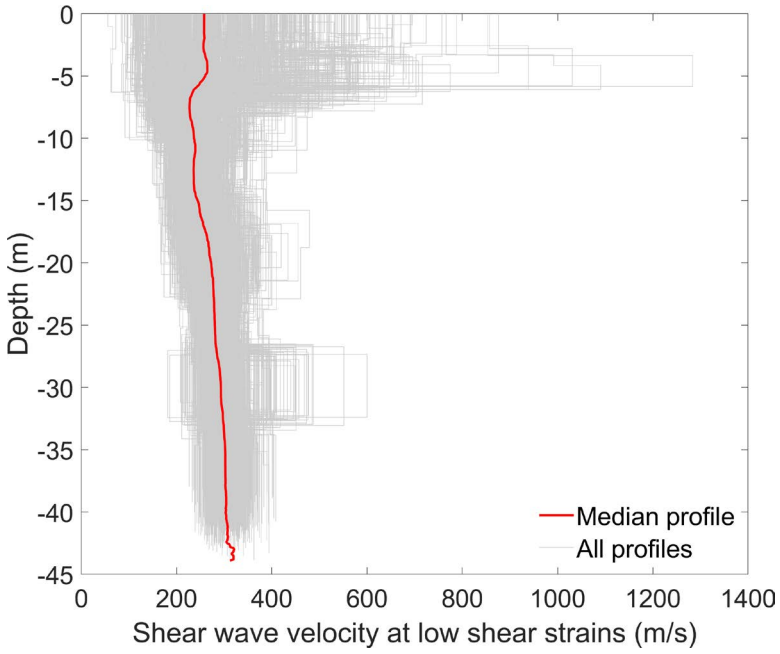

Figure 5. Probabilistic shear wave velocity profiles.

The shear modulus and damping ratio curves utilized in this study were derived from geotechnical properties obtained through laboratory tests and from empirical curves available in the literature. Specifically, for sandy soils, it has been adopted the curves proposed by (Kokusho, 1980; Seed and Idriss, 1970), which have been widely validated for cohesionless soils with similar geotechnical characteristics. These curves take into account for the nonlinear behaviour of sands, particularly at large shear strains, where they capture the effects of grain crushing and contractive tendencies. For clayey soils, it has been used the empirical relationships developed by (Vucetic and Dobry, 1991) which provide a well-established framework for describing the strain-dependent behaviour of cohesive soils as a function of their plasticity index. These curves have been assigned to the different soil layers in the generated models based on their corresponding lithological classification and plasticity characteristics, ensuring a consistent representation of the nonlinear dynamic response of the soil profiles. Note that damping ratio values at low strains, for the analysed materials, vary in a narrow band between 1-1.2 %. In addition, another relevant variable influencing the dynamic properties of the simulated soil profiles is the density. This physical property has been indirectly considered as a random variable by using the relationship proposed in Nakamura, 1989:

$$\gamma = 8.32 \cdot \log_{10} Vs - 1.61 \cdot \log_{10} H \tag{3}$$

where H is the depth in meters; Vs represents shear wave velocity (m/s); γ is the unit weight (kN/m^3). It is worth mentioning that the density plays a central role when assessing multivariate arrangements, as shown below. Figure 6 depicts the random set of density profiles after applying Eq. (3).

Once the probabilistic set of soil features has been generated, the next step is to characterise the seismic hazard at the site. It has been done by considering actual ground motion records acquired in seismic stations. Then, using both soil profiles and ground motion records, the probabilistic propagation of seismic waves has been performed.

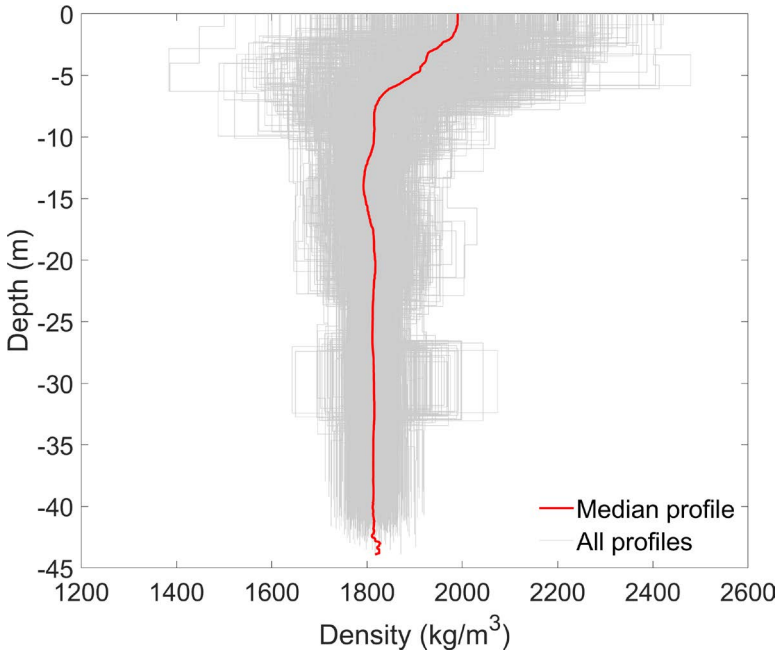

Figure 6. Density of the soil profiles.

3. Seismic hazard characterization

The study of earthquake-induced ground vibrations is a topic of great importance, not only in areas of high seismic hazard, but worldwide. This is due to the fact that, as commented in (Coburn and Spence, 2002), earthquakes with magnitudes around 5.5 Mw can occur almost anywhere in the world (this represents the level of energy that can be released in non-tectonic geological processes). If these events are shallow, it is expected that trigger significant intensities in areas containing vulnerable structures; it may derive in extensive damage. Evidence of this has been provided by (Alarcón and Benito Oterino, 2014), who analysed the negative consequences of two earthquakes on the civil infrastructure of several European cities, particularly Lorca in Spain and Emilia in Italy. What is most notable about these catastrophic events is that the related earthquakes can be considered low-to-moderate magnitude (5.1 and 5.8 Mw, respectively). This situation is not unique to Europe; several regions of the world are highly vulnerable to earthquakes, especially in low-income areas.

To describe the seismogenic environment of the study area, Fig. 7 presents a seismic hazard map of the PGAs and the location of the Port of Barcelona. This figure highlights that the region is characterized by low-to-moderate seismicity, as indicated by the relatively low expected ground accelerations. Despite this, historical records and recent studies emphasize that even regions of low-to-moderate seismic hazard are not exempt from experiencing damaging seismic events, particularly when site effects or local soil conditions amplify ground motions (Coburn and Spence, 2002). In this context, the assessment of earthquake-induced ground vibrations remains a key issue for ensuring the resilience of infrastructure, especially in areas where the combination of vulnerable structures and specific geotechnical conditions may lead to significant damage, even under moderate seismic loads.

In line with the above, instead of using probabilistic seismic hazard calculations to characterize the expected ground motions of the area (Cornell, 1968), which may derive in underestimation of the expected risk (Mulargia et al., 2017), it has been opted to select earthquakes whose magnitude range between 4 and 6 Mw; the maximum hypocentral distance has been set at 10 km. The Engineering Strong Motion Database has been used to select these ground motion records (Luzi et al., 2016). Figure 8 shows the spectra of the 125 signals that met the requirements described above.

Based on this approach, the variability of intensity measures like the PGA can be very large. However, note that only a few ground motions of the set exhibit large PGAs. In order to prove this, a histogram with PGA values has been included in the new version of the manuscript (Fig. 9). In this Figure, it can be seen that more than a half of the PGA values are lower than 0.1 g; more than 85% of the PGAs are lower than 0.2g. Notwithstanding, approximately 6% of the ground motion records exhibit PGA values higher than 0.3 g. This number is consistent with the fact that only 6.4% of the results exceeded the 0.4% shear strain limit, related to the validity of the equivalent linear method, , as shown below.

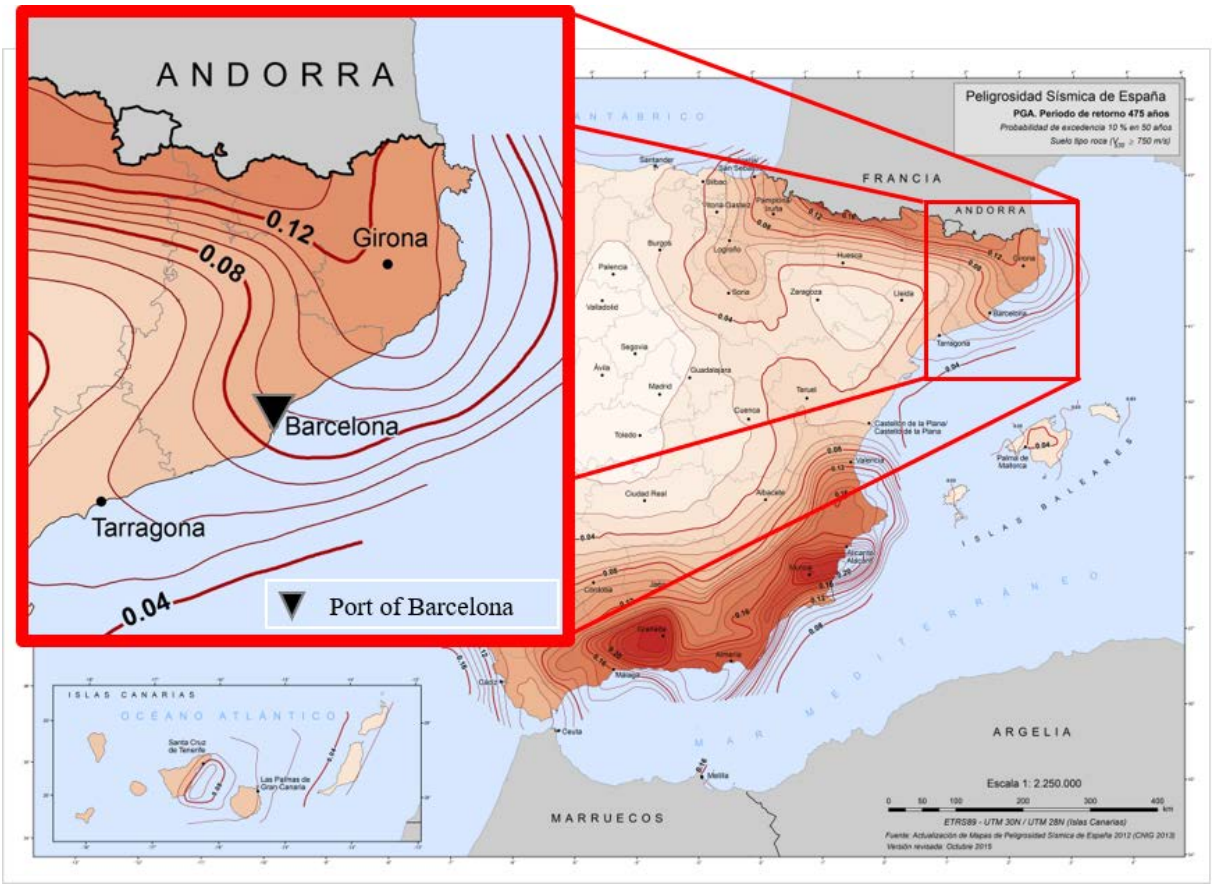

Figure 7. Seismic hazard map and location of the project (IGN, 2012).

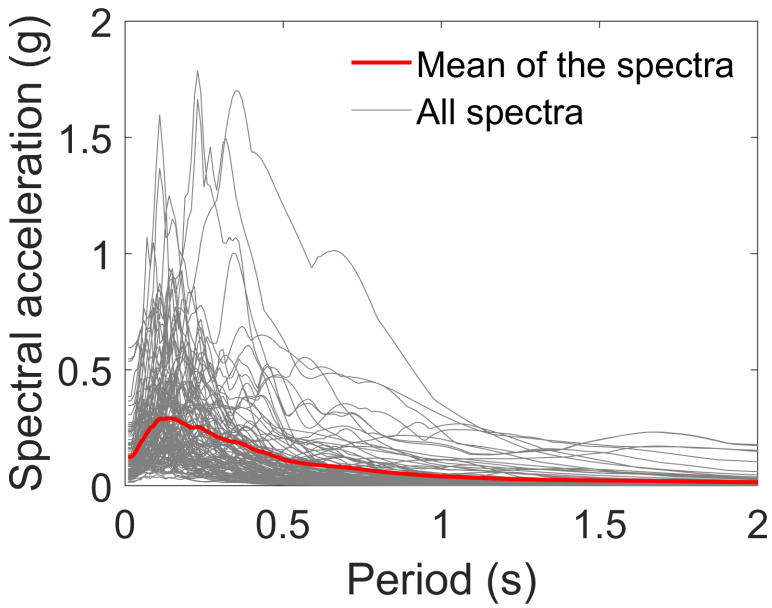

Figure 8. Spectra of 125 selected ground motion records.

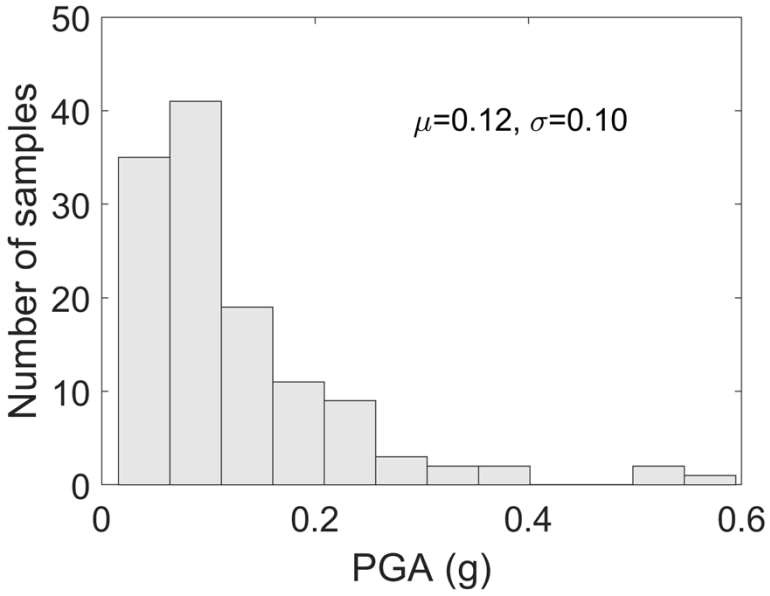

Figure 9. Spectra of 125 selected ground motion records.

4. Degradation of soil properties

Depending on the soil type and depth, the mechanical properties of the soil can be highly modified due to the pass of seismic waves. In this respect, it is a common practice to use simplified 1D soil models to 3D finite-element representations. However, the higher the complexity of the model the higher the computational time involved in solving the dynamic problem. Moreover, due to the boundary conditions related to the reflection of seismic waves in 3D models, it is sometimes necessary to develop large soil models, which significantly increase the number of finite elements. In order to tackle this computational effort, simplified soil representations are widely used to estimate the dynamic response of large simulations. One of the most employed is the 1D model, in which the soil layers are considered as Kelvin-Voigt solids. In brief, this model is represented by a purely viscous damper and elastic spring connected in parallel. Since this model adequately captures the SH waves (Vrettos, 2013), it allows a good approximation of the dynamic response of a soil volume. Moreover, this model has been extended to consider nonlinearities associated to the stiffness degradation of the soil, and the consequent increase in damping ratio due to shear strains. It can be achieved by means of the linear equivalent method (Assimaki et al., 2000). Due to the reduction in terms of computational effort, the 1D model becomes an ideal candidate to include uncertainties via Monte Carlo simulations.

Using the methodology described in Fig. 1, the propagation of seismic waves through the soil profiles is carried out. Figure 10a shows in grey the one-thousand nonlinear wave velocity profiles after the degradation process whilst the red line shows the median profile. Regarding damping ratio (Fig. 10b), it has been observed that, after the propagation process, the median profile is around 5%. Note that the damping ratio tends to increase with depth. It can be related with the materials found in the study zone.

After comparing the fundamental periods of the elastic and inelastic median profiles (see Fig. 11), it can be seen a significant degradation of the stiffness. The median of the ratios between the elongated and elastic periods is around 16%.

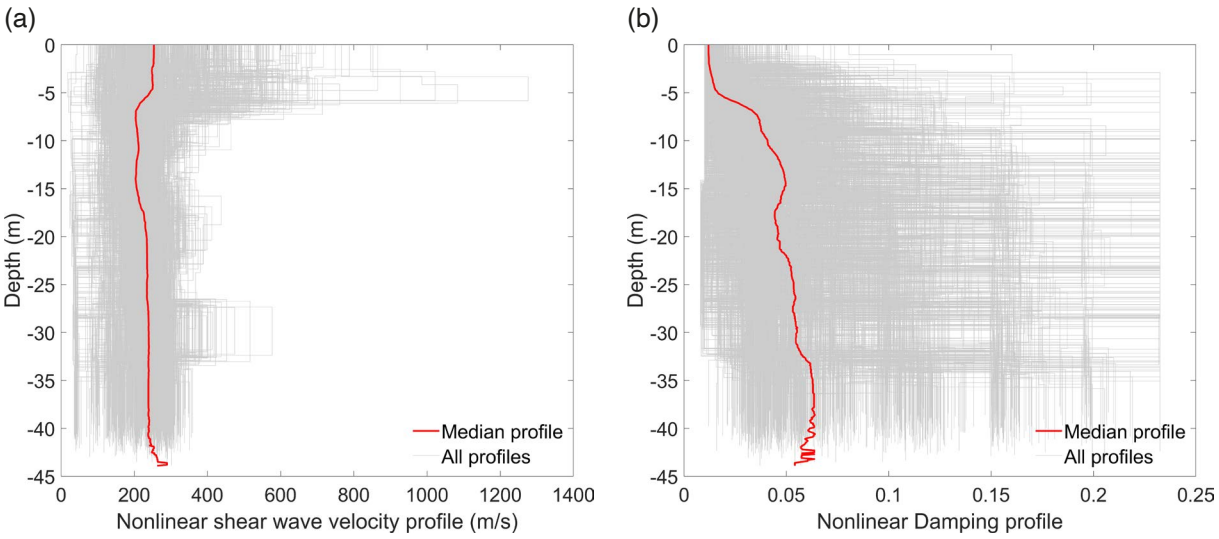

Figure 10. (a) Nonlinear Vs and (b) Nonlinear damping ratio of the one-thousand profiles.

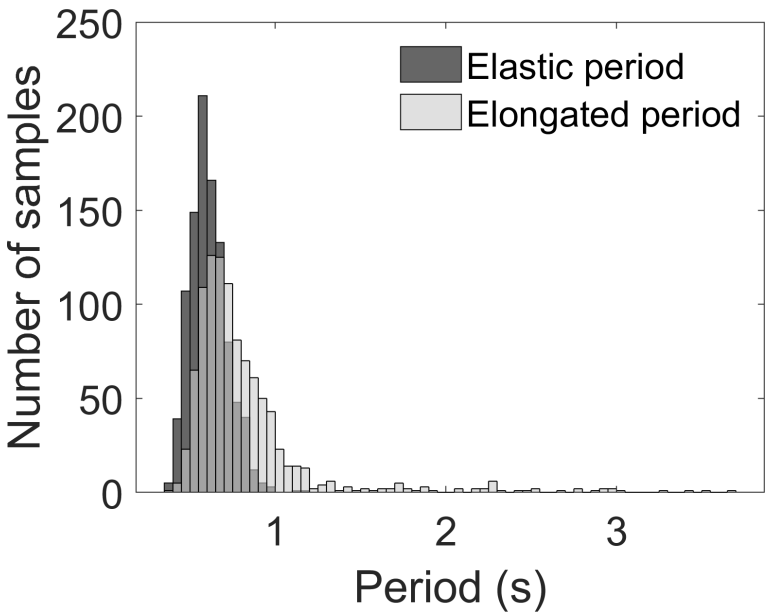

Figure 11. Comparison between the elastic and inelastic fundamental periods.

5. Intensity measures and engineering demand parameters

The relationship between IM and EDPs can be employed to estimate the expected seismic risk of systems. For instance, from a set of IM-EDP pairs, it can be derived fragility functions according to the so-called 'cloud analysis' approach (Jalayer et al., 2015). These functions play a central role in seismic risk assessment, as they condition the probability of exceeding a specific threshold (Generally in terms of EDPs), commonly associated with a level of damage. In the following section, a brief description of IMs and EDPs has been presented.

5.1 Intensity measures

An instrumental IM is a parameter extracted from a ground motion record to characterize seismic hazard (Atkinson and Kaka, 2007). In this article, a set of 18 IMs have been employed. They have been summarized in Table 1; further

details on how to calculate these IMs can be found in Vargas-Alzate et al., 2022. At a first stage, IMs have been used as scalar-based proxies to predict parameters associated to the nonlinear dynamic response of the soil. That is, by performing linear and non-linear regressions, in the log-log space, on the bivariate distributions between IM and EDPs, the IM exhibiting the highest efficiency has been identified. Based on these highly correlated variables, fragility functions have been derived in subsequent sections.

Three types of IMs have been considered in this research. The first type corresponds to IMs derived from the dynamic equilibrium equation for single degree of freedom systems, SDoF:

$$m\ddot{u}(t) + c\dot{u}(t) + ku(t) = -m\ddot{u}_g(t) \tag{4}$$

where $\ddot{u}(t)$, $\dot{u}(t)$ and $u(t)$ are the spectral acceleration, velocity and displacement time history responses of the SDoF, respectively; $\ddot{u}_g(t)$ is the acceleration ground motion; m, c, and k represent the mass, damping ratio and stiffness of the system, respectively. Note that these IMs depend on the fundamental period of the system (T_1), in this case, the soil profile. IMs from 1 to 6 belong to this category. IMs 7 and 8 belong to the second type of IMs, which are extracted from the equivalent velocity spectrum (Benavent-Climent et al., 2004; Cheng et al., 2015; Güllü et al., 2019; Yazgan, 2012); these IMs also depend on T_1. Finally, the third type of IMs, 9 to 18 in Table 1, are calculated from the ground motion record; it means, no spectral transformations have been performed.

ID	Intensity Measure	Variable
1	Spectral acceleration at T_1	$Sa(T_1)$
2	Spectral velocity at T_1	$Sv(T_1)$
3	Spectral displacement at T_1	$Sd(T_1)$
4	Average spectral acceleration	$AvSa$
5	Average spectral velocity	$AvSv$
6	Average spectral displacement	$AvSd$
7	Equivalent velocity at T_1	$VE(T_1)$
8	Average equivalent velocity	$AvVE$
9	Peak ground acceleration	PGA
10	Peak ground velocity	PGV
11	Peak ground displacement	PGD
12	Specific Energy Density	SED
13	Arias intensity	I_A
14	Characteristic intensity	I_C

ID	Intensity Measure	Variable
15	Root mean of the velocity	vel_{RMS}
16	Root mean of the acceleration	acc_{RMS}
17	Cumulative Absolute Velocity	CAV
18	Fajfar intensity	I_F

Table 1. Intensity measures; further details can be found in Vargas-Alzate et al., 2022.

5.2 Engineering demand parameters

EDPs are variables extracted from the dynamic response of systems and can be used to characterize the expected damage. In this article, three EDPs have been analysed; they can be easily connected with damage in soils.

5.2.1 Maximum shear strain reached by any layer of the soil profile, γ_{max}

After performing the seismic wave propagation process, it can be estimated the time history evolution of the displacement at each interface. From this information, and the thickness of the layer, it can be calculated the evolution of the shear strain in time:

$$\gamma_i(t) = \frac{\delta_i(t) - \delta_{i-1}(t)}{h_i} \tag{5}$$

where $\delta_i(t)$ is the time-history displacement at the interface i of the soil profile; h_i represents the thickness of the layer i. Then, the maximum shear strain reached at the layer i, γ_{max_i}, can be calculated as follows:

$$\gamma_{max_i} = max\left(abs\left(\gamma_i(t)\right)\right) \tag{6}$$

Finally, the maximum shear strain in the soil profile, γ_{max}, is given by:

$$\gamma_{max} = max\left[\gamma_{max_1}, \gamma_{max_i} \cdots \gamma_{max_n}\right] \tag{7}$$

5.2.2 Elongation of the fundamental period of the soil profile, δT

The stiffness lost by a soil profile can be estimated by analysing the elongation of the fundamental period after propagation of seismic waves. Thus, by using the values shown in Fig. 11, the ratio between the elongated (T_{el}) and fundamental periods (T_1) has been defined as EDP:

$$\delta T = \frac{T_{el}}{T_1} \tag{8}$$

5.2.3 Resulting damping ratio after the wave propagation, ξ

The degradation process induced by seismic ground motions in soil profiles generally implies an increase of damping ratio. It is more noticeable in loose materials and can be attributed to particle rearrangement. This increase has been measured after the propagation of seismic waves through the soil profiles. That is, the resulting damping ratio at the end of the iterative process associated with the linear equivalent analysis, ξ, has also been used as EDP.

6. Causality analysis based on bivariate and multivariate distributions

IM-EDP bivariate and multivariate ($\vec{V}$IM-EDP) distributions can be statistically characterized by performing a linear and a nonlinear regression analysis in the log-log space. In this sense, the following general linear least-square model allows several types of regressions:

$$y = \alpha_0 + \sum_{i=1}^{N_{IV}} \sum_{j=1}^{n} \alpha_{j+(i-1)*n} z_j + \varepsilon \tag{9}$$

where N_{IV} represents the number of information variables (IV) considered in the regression model; n stands for the polynomial degree; $\alpha_0, \alpha_1, \ldots \alpha_{N_{IV}*n}$ are the scalars maximizing the coefficient of determination, R^2, between model and data; z_j are basic functions; ε represents the residuals. It can easily be seen how a polynomial regression falls within this model, that is, $z_1 = x, z_2 = x^2 \ldots z_n = x^n$. Substituting in Eq. (10) $y = \ln EDP$ and $z_j = (\ln IV_i)^j$, the general linear least-square model using polynomial functions can be used to extract statistical information from IM-EDP pairs according to the following equation:

$$\ln EDP = \alpha_0 + \sum_{i=1}^{N_{IV}} \sum_{j=1}^{n} \alpha_{j+(i-1)*n} (\ln IV_i)^j + \varepsilon \tag{10}$$

This equation allows multi-linear ($n = 1$) and -quadratic ($n = 2$) regression models in the log-log space. In this way, several sources of information can be considered simultaneously to better predict a specific EDP. R^2 has been used herein to provide an estimation of the variability when analysing IM-EDPs pairs. That is, the higher R^2, the lower the variability when predicting some EDP given an IM. Consequently, the IM providing the highest R^2 is the most efficient. Two types of polynomials have been used to calculate R^2. It means, $n = 1$ and $n = 2$ have been replaced in Eq. (10), providing two coefficients of determination, R_L^2 and R_{NL}^2, where subscript L stands for linear and NL for non-linear. The reason for considering a non-linear regression model is that, in some cases, the IM-EDP bivariate distribution cannot be properly described by using linear functions, even in the log-log space. Further information regarding the development and implementation of this type of polynomial models in the log-log space can be found in Chapra (2018).

6.1 Bivariate distributions

There are several ways to derive fragility functions by using IM-EDP pairs. Note that these curves are used to define the probability of exceedance a given damage threshold. The latter is a specific value of the EDP under consideration. For instance, cloud analysis (Jalayer et al., 2015) requires to calculate the best fit curve between a set of IM-EDPs realizations in the log-log space. The resultant curve is used to estimate the median of a parametric statistical distribution, given an IM value. The variability of this parametric distribution is estimated as the logarithmic standard deviation of the residuals ($S_{y/x}$). In this way, the conditional probability of exceeding a certain damage threshold, given an IM value, can be calculated. In the following, variables described in section 5.1 has been used as IMs, and γ_{max}, δT and ξ (see Section 5.2) as EDPs.

6.1.1 Maximum shear strain

Figure 12 presents 18 clouds of IM-γ_{max} data points. The results indicate that PGV exhibits the strongest correlation, with values of 0.756 for the linear regression and 0.759 for the quadratic regression; the one with the lowest correlation has been the CAV with values between 0.446 for the linear and 0.447 for the non-linear regression. It is important to note that data points where $\gamma_{max} > 0.4\%$ have been excluded from the statistical

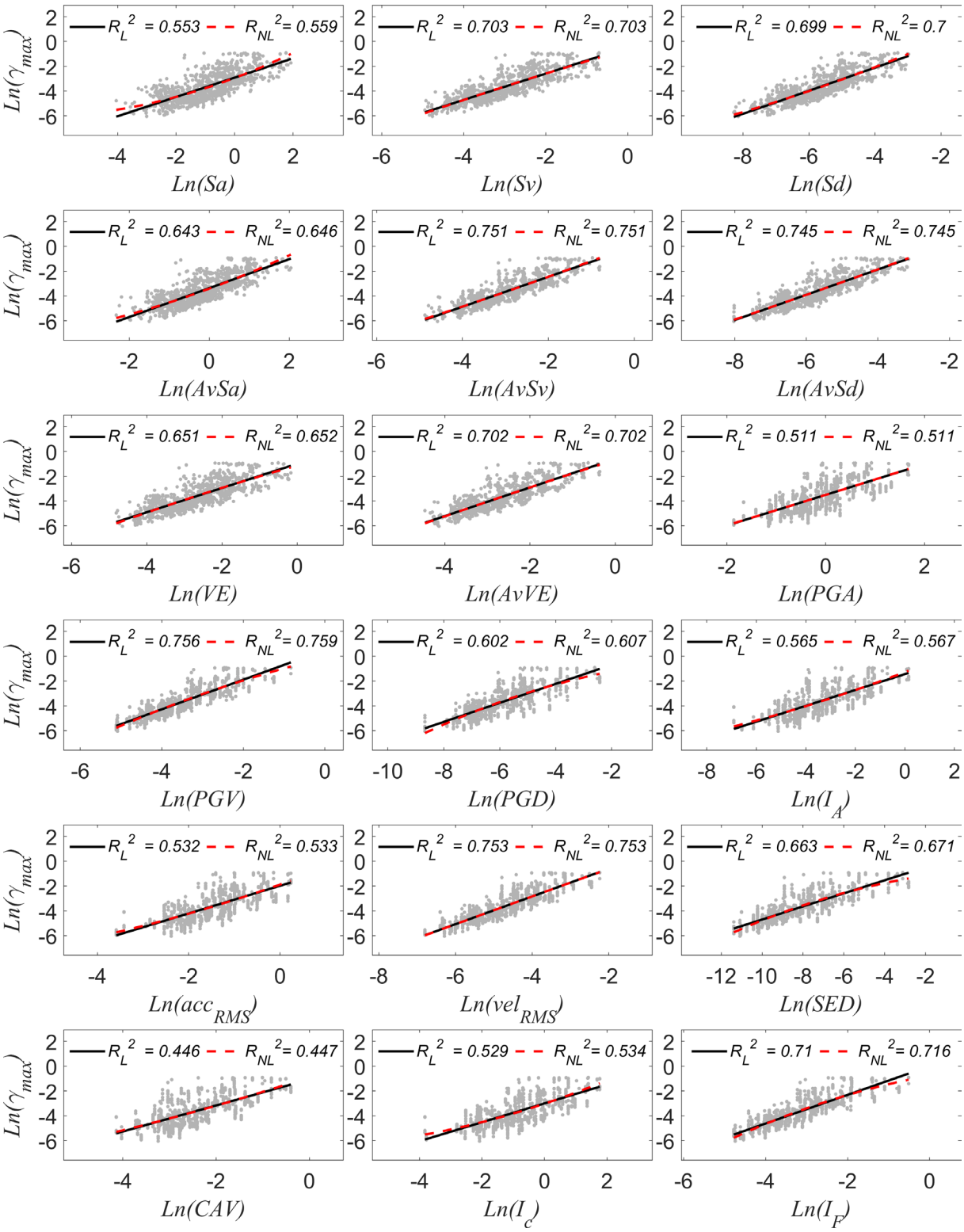

Figure 12. IM-γ_{max} clouds – Bivariate analysis.

analysis, as the equivalent linear method cannot accurately capture the nonlinear soil response at these deformation levels. In this range, soil stiffness degradation and hysteretic energy dissipation become highly nonlinear, leading to potential underestimation of the response when using an equivalent linear approach. Overall, there are no significant differences between the linear and quadratic regression models, suggesting that the relationship between PGV and γ_{max} can be reasonably approximated using a linear fit.

Although PGV is the IM most correlated with γ_{max}, AvSv has been selected for the derivation of fragility functions. On the one hand, due to the fact that this IM depends on T_1, on the other hand, it appears in the causality analysis considering the multivariate distributions, which are explained in section 6.2. Thus, by using AvSv-γ_{max} pairs, the probability of exceeding $\gamma_{max} = 0.1\%$ has been estimated (see Fig. 13). This damage threshold generally corresponds to a loss of soil stiffness around 50%, which can be seen as a severe damage state.

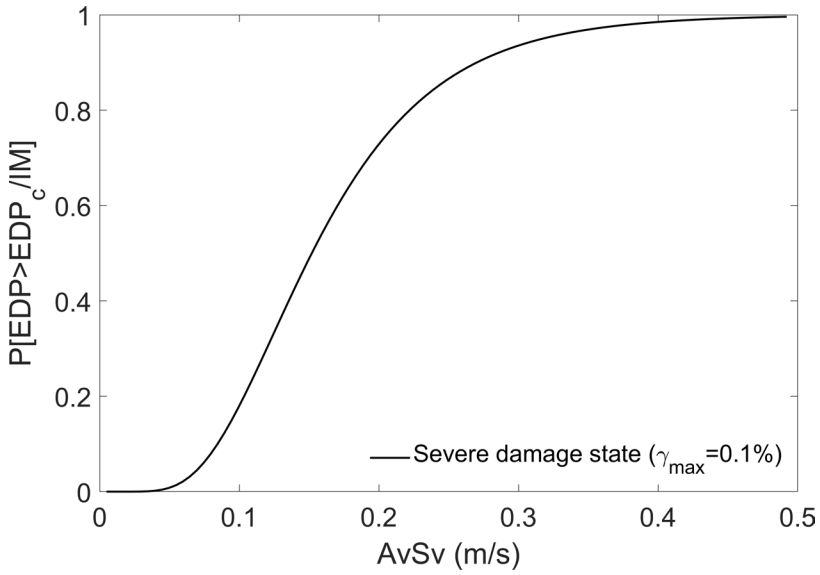

Figure 13. Fragility curve for $\gamma_{max} = 0.1\%$.

6.1.2 Elongation of the fundamental period

In this case, the most efficient intensity measure (IM) is AvSd, for which the regression analysis has been better characterized by the quadratic model. This suggests that the relationship between AvSd and δT exhibits a nonlinear trend (Fig. 14), making the quadratic fit more suitable for capturing the underlying behaviour.

Based on the AvSd-δT data pairs, the probability of exceeding a fundamental period elongation of 20% has been estimated (see Fig. 15). The results indicate that, for very low values of AvSd, the probability of reaching this elongation level is relatively high. This behaviour could be attributed to the inherent variability in structural and soil responses at low excitation levels, where small increments in IM may lead to noticeable changes in δT due to initial stiffness degradation effects. These findings highlight the relevance of AvSd as a predictor of period elongation, which is a key parameter for assessing structural damage and soil-structure interaction effects.

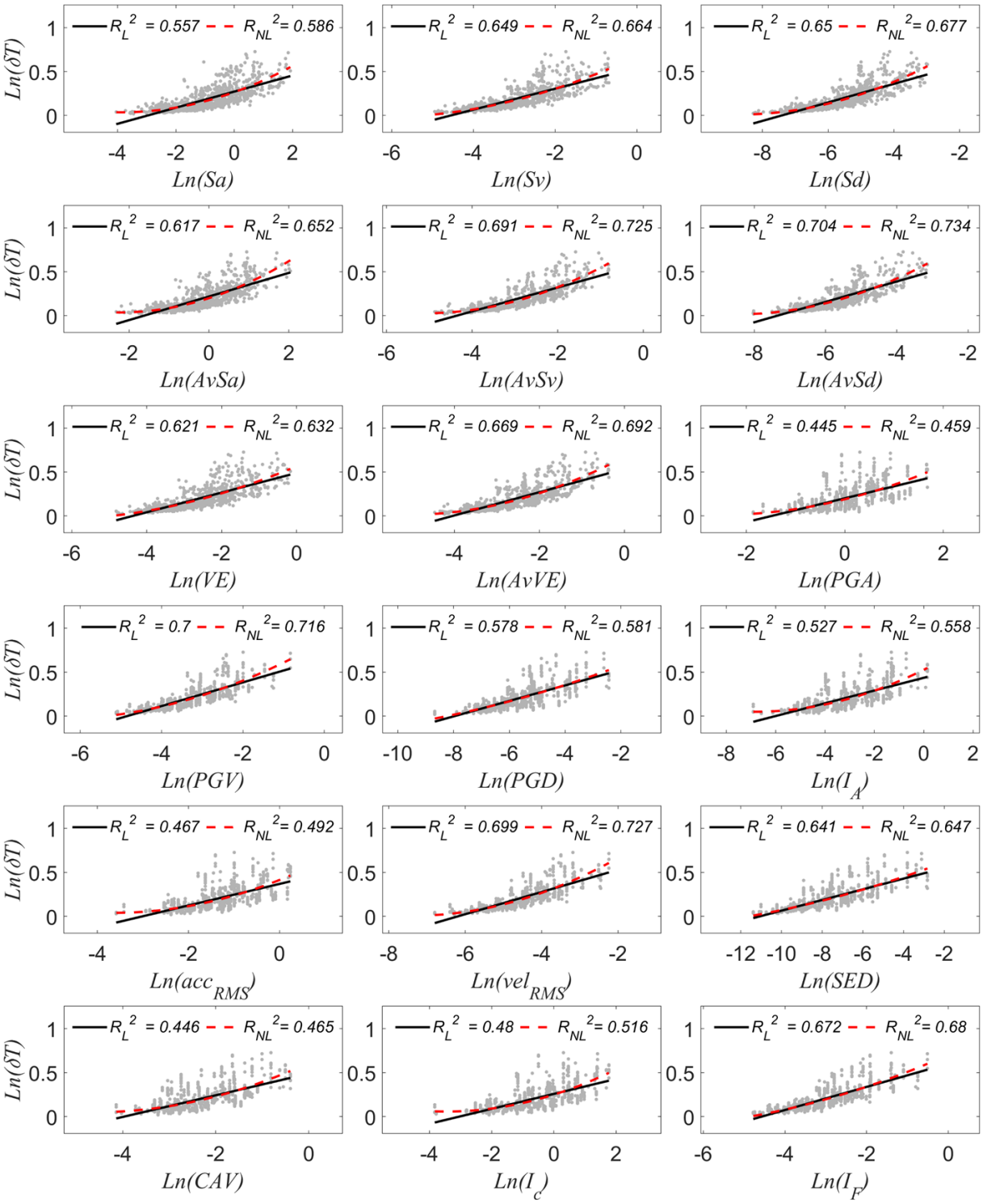

Figure 14. IM-δT clouds – Bivariate analysis.

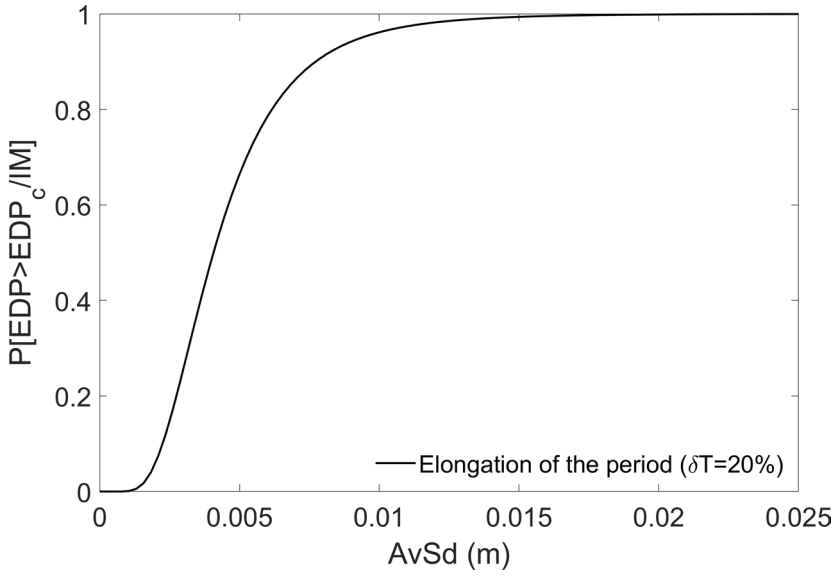

Figure 15. Fragility curve for $\delta T = 20\%$.

6.1.3 Increase of damping ratio

The degradation of the soil stiffness produces an increase of damping. In this section, the final damping ratio, ξ, obtained at the end of the iterative wave propagation procedure has been analysed. The results indicate that ξ can reach values of approximately 20%, which is likely associated with the most intense ground motions in the selected dataset. This increase of damping is expected, as stronger seismic excitations induce higher shear strains, resulting in greater energy dissipation.

Figure 16 presents the 18 clouds of IM-ξ data pairs. Similar to the results observed for δT, AvSd has been identified as the most efficient intensity measure (IM) for predicting ξ. However, no significant differences have been found between the linear and nonlinear regression models, suggesting that both provide comparable levels of accuracy.

Based on the most correlated data pairs (AvSd-ξ), the probability of the final damping ratio exceeding 5% has been estimated (see Fig. 17). The results indicate that, for very low values of AvSd, the probability of reaching or surpassing this damping ratio threshold is relatively high. This behaviour could be attributed to the inherent variability in damping at low excitation levels, where small changes in IM may lead to substantial changes in ξ due to the sensitivity of the damping mechanisms in this range.

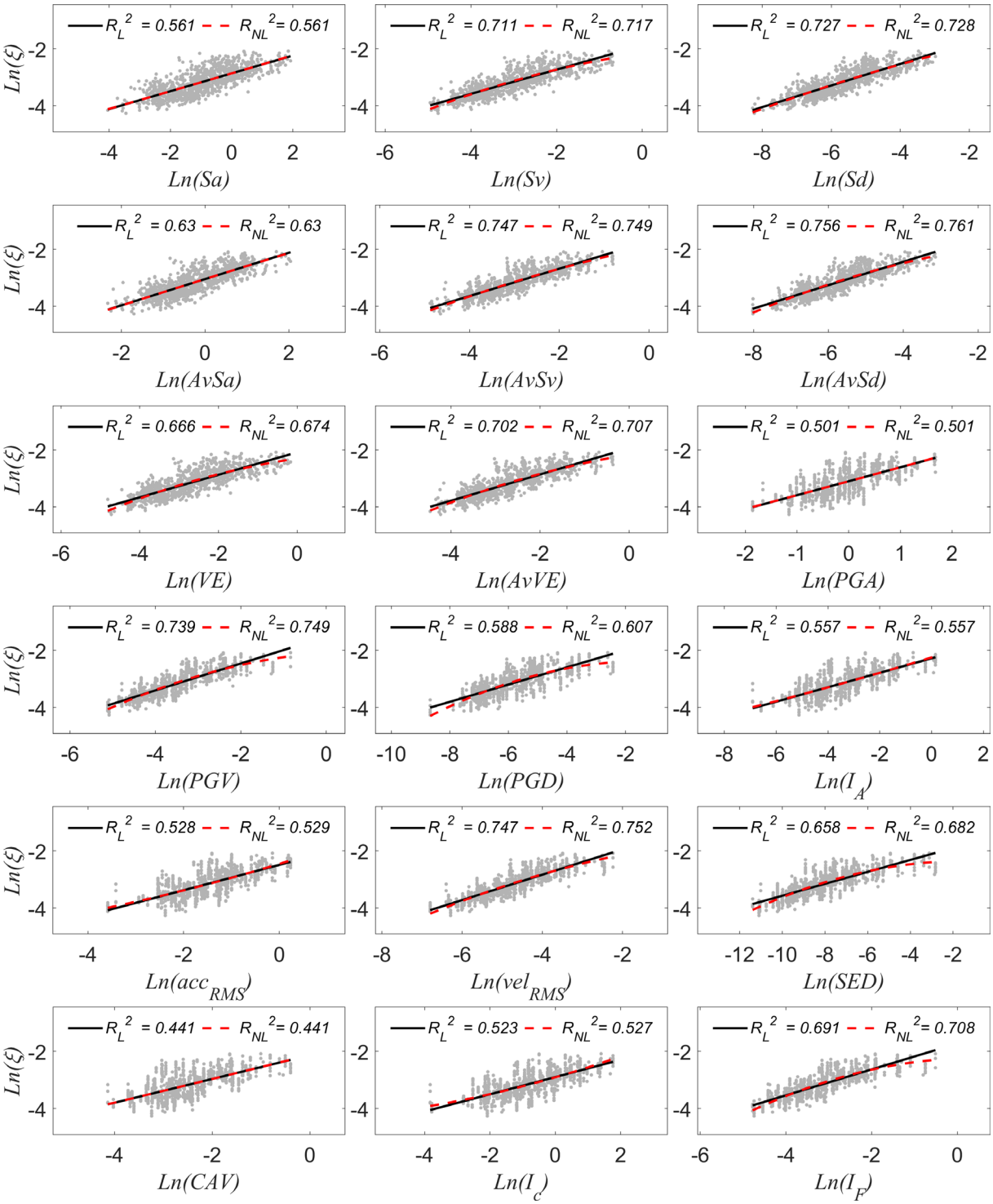

Figure 16. IM-ξ clouds – Univariate analysis.

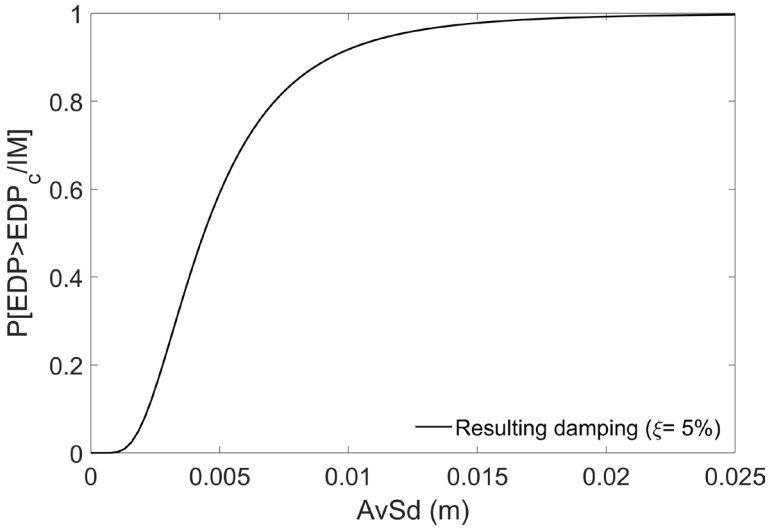

Figure 17. Fragility curve for exceeding a 5% of damping ratio.

Fragility function derived so far only employs information from a single scalar-based IM. However, several researchers have proven that augmenting the number of information variables generally derives in an increase of efficiency (Ebrahimian et al., 2015). In fact, common approaches to assessing the vulnerability of structures typically produce fragility curves based on a single intensity measure, as the procedure described in this section. However, seismic action is complex, and relying on a single parameter may overlook other critical characteristics of ground motion (Gehl et al., 2011; Seyedi et al., 2010). In the next section, fragility surfaces have been developed, which represent the probability of damage as a function of multiple parameters, providing a more comprehensive interpretation of the uncertainties associated with the hazard characterization.

6.2 Multivariate distributions

As commented above, Eq. (10) allows identifying enhancing arrangements that consider statistical information from several IVs. To do so, it is necessary to replace in this equation N_{IV} for the desired number of IVs. In the present study, $N_{IV} = 2$ has been tested. Then, R^2 has been calculated considering the multi-regression model that allows combining information provided by the soil profile and the IMs. Several soil information variables have been included in the identification of the most correlated $\vec{V}$IMs. A description of these variables is presented in Table 2.

Variables	Equation	Description
T_{S_L}	$\sum_{i=1}^{nlayer} T_{S_{L,i}}$	Fundamental period of the soil profile
$\bar{\xi}_L$	$\frac{\sum_{i=1}^{nlayer} \xi_{L,i}}{nlayer}$	Average linear damping of the soil profile
$\bar{\rho}_S$	$\frac{\sum_{i=1}^{nlayer} \rho_{S,i}}{nlayer}$	Average density of the soil profile
$\overline{Vs_L}$	$\frac{\sum_{i=1}^{nlayer} Vs_{L,i}}{nlayer}$	Average shear wave velocity of the soil profile

Table 2. Intensity measures.

The following sections present and analyse the results obtained by considering a multivariable distribution for predicting γ_{max}, δT and ξ. These analyses provide a more robust understanding of the dynamic behaviour of the system. It is worth mentioning that the number of IVs is 22, consequently, 231 different $\vec{V}$IMs have been statistically analysed.

6.2.1 Maximum shear strain

For the multivariate analysis, results from linear (a) and quadratic (b) regression models for γ_{max} has been compared in Fig. 18. It can be observed that, for the case of γ_{max}, the variables $AvSv$ and $\bar{\rho}_S$ are the pair exhibiting the highest efficiency. Compared to the results obtained from the bivariate analysis, employing a multivariate approach improves the correlation from 0.751 to 0.796 in the linear case and from 0.751 to 0.8 in the quadratic case. The fragility surface (see Fig. 19) for exceeding $\gamma_{max} = 0.1\%$ (which can be tied to a severe damage threshold) provides a more comprehensive representation of the complex interactions between seismic parameters and soil response.

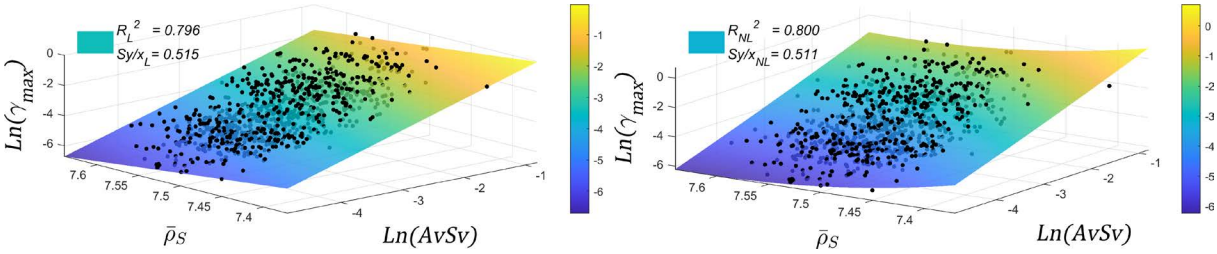

Figure 18. IM-γ_{max} clouds – Multivariate analysis. (a) linear and (b) quadratic regression.

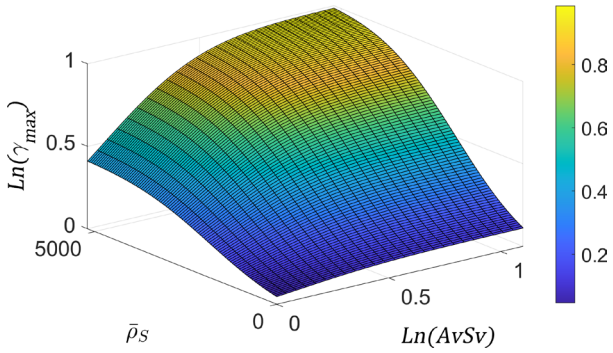

Figure 19. Fragility surface for $\gamma_{max} = 0.1\%$.

6.2.2 Elongation of the fundamental period

For the case of δT, it has been observed an improvement in causality when compared to the bivariate analysis. The variable $AvSd$ is a component of the $\vec{V}$IM most correlated, paired with PGV in the linear regression and with acc_{RMS} in the quadratic regression. Regarding the correlation values, there is an increase from 0.704 to 0.729 (Fig. 20b) for the linear case and from 0.734 to 0.762 for the quadratic case (Fig. 20b). Figure 21 shows the fragility surface for δT given the quadratic case.

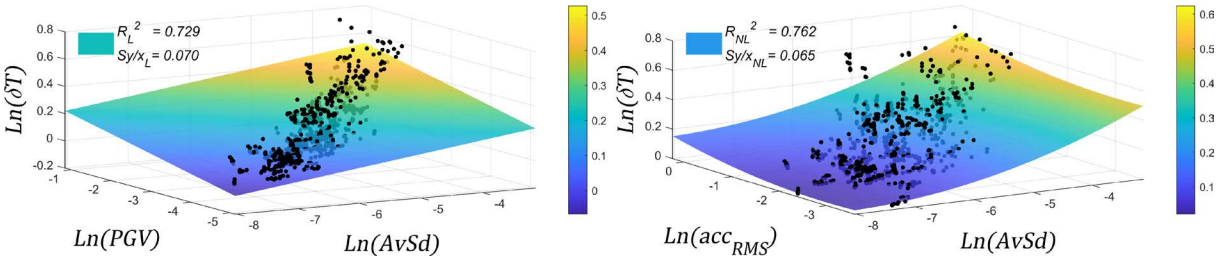

Figure 20. IM-δT clouds – Multivariate analysis. (a) linear and (b) quadratic regression.

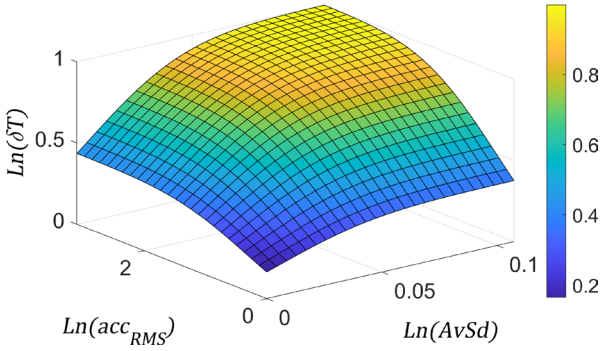

Figure 21. Fragility surface for δT.

6.2.3 Increase of damping ratio

For ξ, similar to the previous cases, an increase in correlation has been observed for both linear and quadratic models. The correlation improves from 0.756 to 0.807 in the linear case (Fig. 22a) and from 0.761 to 0.810 in the quadratic case (Fig. 22b), resulting in the scenario with the highest correlation observed. In addition, the fragility surface for exceeding the 5% damping ratio has been derived (Fig. 23), providing a detailed representation of the probability of exceeding this threshold.

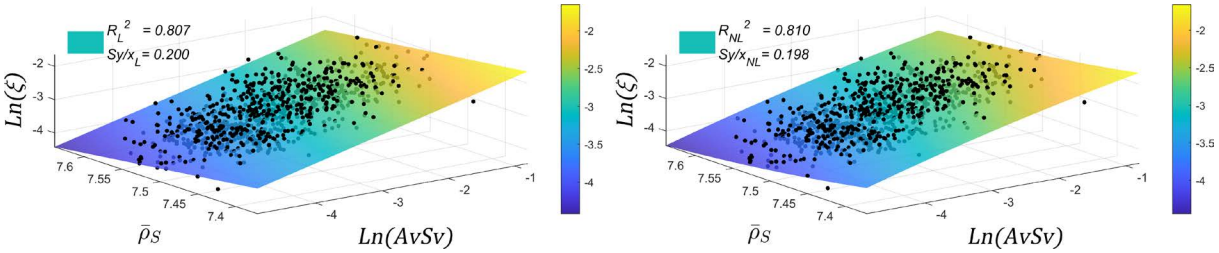

Figure 22. IM-ξ clouds – Multivariate analysis. (a) linear and (b) quadratic regression.

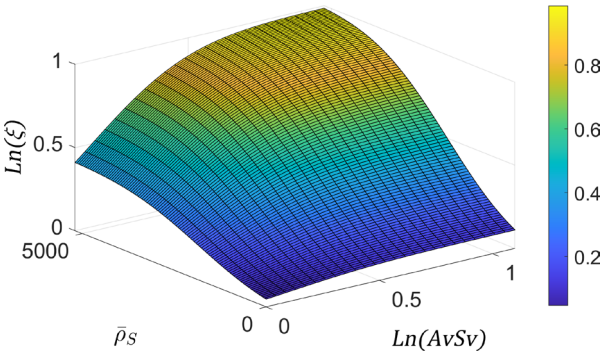

Figure 23. Fragility surface for ξ.

7. Conclusion

This study highlights the importance of properly characterising site effects for robust seismic risk assessment, recognising the complexity of the variables involved. The application of a computational framework for assessing the probabilistic dynamic response of soils in the Port of Barcelona, essentially using information from seismic dilatometer Marchetti test (SDMT), has provided valuable insights. The incorporation of new advances in this computational framework has been aimed at addressing the complexity of soil dynamic characterisation.

An approach to seismic hazard characterisation, based on ground motion records with specific magnitudes rather than PSHA-based estimates, has been adopted to reduce the risk of underestimating seismic hazard, commonly observed in non-seismic regions (Silva et al., 2016). Moreover, quantification of inelastic ground response using the equivalent linear method further improves the accuracy of the analysis.

Two types of approaches have been proposed for this study. The first involves a bivariate analysis aimed at identifying the optimal IM-EDP pair to estimate the probability of exceeding specific damage thresholds. In this approach, fragility curves have been derived for each of the EDPs selected.

The second approach proposes the use of multiple intensity measures and soil parameters ($\vec{V}$IMs) to predict the EDP. Incorporating several variables has been shown to yield stronger correlations, allowing the identification of an optimal set of $\vec{V}$IMs. Using these vectors, fragility surfaces have been developed, providing a more detailed and comprehensive depiction of expected soil damage compared to traditional fragility curves.

While bivariate analysis effectively identifies the best IMs for predicting specific EDPs, the multivariate approach offers a more advanced framework, especially for estimating the probability of exceeding damage thresholds. In this way, the relationships between seismic inputs and ground responses are captured more effectively. Note that, compared to the bivariate method, the multivariate approach achieves superior correlation values, demonstrating enhanced predictive accuracy and reduced uncertainty. For instance, in this study, transitioning from bivariate to multivariate analysis significantly increased correlation coefficients, emphasizing the advantages of integrating additional parameters. This underlines the importance of addressing the complex and multidimensional nature of seismic actions in hazard characterisation and vulnerability assessment.

Despite the advances presented in this study, certain limitations should be acknowledged. The proposed computational framework has been applied to a specific case study, and its generalization to other sites requires further validation with additional real-case applications. The methodology relies on the availability of high-quality in situ geotechnical and geophysical data, which may not always be accessible in different study areas. Additionally, while the use of ground motion records with specific magnitudes mitigates the underestimation of seismic hazard, future studies could explore the integration of site-specific probabilistic seismic hazard analyses (PSHA) to further enhance the accuracy of the input motions. Moreover, the equivalent linear approach employed in this study, while effective for moderate strain levels, presents limitations in capturing highly nonlinear soil behaviour under extreme loading conditions. Addressing these aspects in future research will contribute to refining the proposed approach and extending its applicability to a broader range of seismic scenarios.

Overall, these results contribute to a more refined and comprehensive understanding of soil dynamics under seismic actions. They support the advancement of methodologies that integrate cutting-edge computational techniques with innovative frameworks for hazard characterization, ultimately improving seismic risk assessment and mitigation strategies.

Acknowledgements. The authors are grateful for the financial support of the Spanish Research Agency (AEI) through the project TED2021-132559B-I00-J-02970 and to Miguel A. Pindado and Ramón Griell of the Autoritat Portuària de Barcelona for the financial support and for providing us with the test results.

References

Alarcón, E. and M. B. Benito Oterino (2014). Foreword special issue LORCA's earthquake, Bull. Earthq. Eng., 12, 1827-1829, doi:10.1007/s10518-014-9602-4.

Amoroso, S., P. Monaco and D. Marchetti (2012). Use of the Seismic Dilatometer (SDMT) to estimate in situ G-γ decay curves in various soil types, in Geotechnical and Geophysical Site Characterization, 4, Coutinho and Mayne (Eds.), Taylor & Francis Group, London, ISBN:978-0-415-62136-6.

Andrus, R. D. and K. H. Stokoe II (2000). Liquefaction Resistance of Soils from Shear-Wave Velocity, J. Geotech. Geoenviron. Eng., 126, 1015-1025, doi:10.1061/(ASCE)1090-0241(2000)126:11(1015).

Angelini, M. E. and G. B. M. Heuvelink (2018). Including spatial correlation in structural equation modelling of soil properties, Spat. Stat., 25, 35-51, doi:10.1016/j.spasta.2018.04.003.

API (2014). Recommended practice 2GEO, Geotechnical and Foundation Design Considerations, 22nd edition, American Petroleum Institute, Washington, RP2A-WSD.

Assimaki, D., E. Kausel and A. Whittle (2000). Model for Dynamic Shear Modulus and Damping for Granular Soils, J. Geotech. Geoenviron. Eng., 126, 859-869, doi:10.1061/(ASCE)1090-0241(2000)126:10(859).

Atkinson, G. M. and S. I. Kaka (2007). Relationships between Felt Intensity and Instrumental Ground Motion in the Central United States and California, Bull. Seismol. Soc. Am., 97, 497-510, doi:10.1785/0120060154.

Baker, J. W. (2007). Probabilistic structural response assessment using vector-valued intensity measures, Earthq. Eng. Struct. Dyn., 36, 1861-1883, doi:10.1002/eqe.700.

Benavent-Climent, A., H. Akiyama, F. López-Almansa and L. G. Pujades (2004). Prediction of ultimate earthquake resistance of gravity-load designed RC buildings, Eng. Struct., 26, 1103-1113, doi:10.1016/j.engstruct.2004.03.011.

Bojórquez, E., I. Iervolino, A. Reyes-Salazar and S. E. Ruiz (2012). Comparing vector-valued intensity measures for fragility analysis of steel frames in the case of narrow-band ground motions, Eng. Struct., 45, 472-480, doi:10.1016/j.engstruct.2012.07.002.

BSSC (2021). NEHRP Recommended provisions for seismic regulations for new buildings and other structures, FEMA, 88 ed., Building Seismic Safety Council, 507-513.

Carrière, S. R., D. Jongmans, G. Chambon, G. Bièvre et al. (2018). Rheological properties of clayey soils originating from flow-like landslides, Landslides, 15, 1615-1630, doi:10.1007/s10346-018-0972-6.

Castellaro, S., F. Mulargia and P. L. Rossi (2008). Vs30: Proxy for Seismic Amplification?, Seismol. Res. Lett., 79, 540-543, doi:10.1785/gssrl.79.4.540.

Chapra, S. C. (2018). Applied numerical methods with MATLAB for engineers and scientists, 4 ed., McGraw-Hill Education, New York, 697, ISBN:978-0-07-339796-2.

Cheng, Y., A. Lucchini and F. Mollaioli (2015). Correlation of elastic input energy equivalent velocity spectral values, Earthq. Struct., 8, 957-976, doi:10.12989/eas.2015.8.5.957.

Coburn, A. and R. Spence (2002). Earthquake Protection, John Wiley & Sons Ltd, Chichester, UK, doi:10.1002/0470855185.

Cornell, C. A. (1968). Engineering seismic risk analysis, Bull. Seismol. Soc. Am., 58, 1583-1606, doi:10.1785/BSSA0580051583.

Cruz, C. and E. Miranda (2021). Insights into damping ratios in buildings, Earthq. Eng. Struct. Dyn., 50, 916-934, doi:10.1002/eqe.3356.

Ebrahimian, H., F. Jalayer, A. Lucchini, F. Mollaioli et al. (2015). Preliminary ranking of alternative scalar and vector intensity measures of ground shaking, Bull. Earthq. Eng., 13, 2805-2840, doi:10.1007/s10518-015-9755-9.

Fajfar, P., T. Vidic and M. Fischinger (1990). A measure of earthquake motion capacity to damage medium-period structures, Soil Dyn. Earthq. Eng., 9, 236-242, doi:10.1016/S0267-7261(05)80002-8.

Farlie, D. J. G. (1960). The Performance of Some Correlation Coefficients for a General Bivariate Distribution, Biometrika, 47, 307, doi:10.2307/2333302.

Gehl, P., S. Sy and D. Seyedi (2011). Developing fragility surfaces for more accurate seismic vulnerability assessment of masonry buildings, in ECCOMAS Thematic Conference On Computational Methods in Structural Dynamics and Earthquake Engineering, COMPDYN, Corfu, Greece, 154.

Güllü, A., E. Yüksel, C. Yalçın, A. Anıl Dindar et al. (2019). An improved input energy spectrum verified by the shake table tests, Earthq. Eng. Struct. Dyn., 48, 27-45, doi:10.1002/eqe.3121.

Hardin, B. O. and G. D. Scott (1967). Erratum for Generalized Kelvin-Voigt Used in Soil Dynamics Study, J. Eng. Mech. Div., 93, 79-79, doi:10.1061/JMCEA3.0000830.

IGN (2012). Actualización de mapas de peligrosidad sísmica de España, Madrid, 267, doi:10.7419/162.05.2017.

Jalayer, F., R. De Risi and G. Manfredi (2015). Bayesian Cloud Analysis: Efficient structural fragility assessment using linear regression, Bull. Earthq. Eng., 13, 1183-1203, doi:10.1007/S10518-014-9692-Z.

Kokusho, T. (1980). Cyclic Triaxial Test of Dynamic Soil Properties for Wide Strain Range, Soils Found., 20, 45-60, doi:10.3208/sandf1972.20.2_45.

Kroese, D. P. and R. Y. Rubinstein (2012). Monte Carlo methods, Wiley Interdiscip. Rev. Comput. Stat., 4, 48-58, doi:10.1002/wics.194.

Luzi, L., R. Puglia, E. Russo and ORFEUS Working Group 5 (2016). Engineering Strong Motion Database, version 1.0. Istituto Nazionale di Geofisica e Vulcanologia, Observatories and Research Facilities for European Seismology, doi:10.13127/ESM.

Marchetti, D. (2018). Dilatometer and Seismic Dilatometer Testing Offshore: Available Experience and New Developments, Geotech. Test. J., 41, 20170378, doi:10.1520/GTJ20170378.

Marchetti, S. (1980). In Situ Tests by Flat Dilatometer, J. Geotech. Eng. Div., 106, 299-321, doi:10.1061/AJGEB6.0000934.

Marchetti, S., D. Marchetti and F. Villalobos (2013). El Dilatómetro Sísmico SDMT para ensayos de suelos in situ, Obras y proyectos, 20-29, doi:10.4067/S0718-28132013000100002.

Mulargia, F., P. B. Stark and R. J. Geller (2017). Why is Probabilistic Seismic Hazard Analysis (PSHA) still used?, Phys. Earth Planet. Inter., 264, 63-75, doi:10.1016/j.pepi.2016.12.002.

Nakamura, Y. (1989). A method for dynamic characteristics estimation of subsurface using microtremor on the ground surface, Railway Technical Research Institute, Tetsudo Gijutsu Kenkyujo, 30, 1, 25-33.

Okur, D. V. and A. Ansal (2007). Stiffness degradation of natural fine grained soils during cyclic loading, Soil Dyn. Earthq. Eng., 27, 843-854, doi:10.1016/j.soildyn.2007.01.005.

Pinzón, L. A., Y. F. Vargas-Alzate, L. G. Pujades and S. A. Diaz (2020). A drift-correlated ground motion intensity measure: Application to steel frame buildings, Soil Dyn. Earthq. Eng., 132, 106096, doi:10.1016/j.soildyn.2020.106096.

Pitilakis, D. and C. Petridis (2022). Fragility curves for existing reinforced concrete buildings, including soil-structure interaction and site amplification effects, Eng. Struct., 269, 114733, doi:10.1016/j.engstruct.2022.114733.

Reed, J. W. and R. P. Kassawara (1990). A criterion for determining exceedance of the operating basis earthquake, Nucl. Eng. Des., 123, 387-396, doi:10.1016/0029-5493(90)90259-Z.

Seed, H. B. and I. M. Idriss (1970). Soil Moduli and Damping Factors for Dynamic Response Analyses, Technical Report, EERRC-70-10, Berkeley, CA.

Seyedi, D. M., P. Gehl, J. Douglas, L. Davenne et al. (2010). Development of seismic fragility surfaces for reinforced concrete buildings by means of nonlinear time-history analysis, Earthq. Eng. Struct. Dyn., 39, 91-108, doi:10.1002/eqe.939.

Silva, V., H. Crowley and P. Bazzurro (2016). Exploring Risk-Targeted Hazard Maps for Europe, Earthq. Spectra, 32, 1165-1186, doi:10.1193/112514eqs198m.

Silva, W. J., N. Abrahamson, G. Toro and C. Constantino (1996). Description and validation of the stochastic ground motion model, Pacific Engineering and Analysis, El Cerrito, CA.

Toro, G. R. (2022). Uncertainty in Shear-Wave Velocity Profiles, J. Seismol., 26, 713-730, doi:10.1007/s10950-022-10084-x.

Vanmarcke, E. H. (1977). Probabilistic Modeling of Soil Profiles, J. Geotech. Eng. Div., 103, 1227-1246, doi:10.1061/AJGEB6.0000517.

Vargas-Alzate, Y. F., A. H. Barbat, L. G. Pujades, L. A. Pinzón et al. (2024). Characterization of free-field seismic motions for soil-structure interaction analysis of nuclear structures using enhanced transfer functions, Soil Dyn. Earthq. Eng., 179, 108494, doi:10.1016/j.soildyn.2024.108494.

Vargas-Alzate, Y. F., J. E. Hurtado and L. G. Pujades (2022). New insights into the relationship between seismic intensity measures and nonlinear structural response, Bull. Earthquake Eng., 20, 2329-2365, doi:10.1007/s10518-021-01283-x.

Vrettos, C. (2013). Dynamic response of soil deposits to vertical SH waves for different rigidity depth-gradients, Soil Dyn. Earthq. Eng., 47, 41-50, doi:10.1016/j.soildyn.2012.04.003.

Vucetic, M. and R. Dobry (1991). Effect of Soil Plasticity on Cyclic Response, J. Geotech. Eng., 117, 89-107, doi:10.1061/(ASCE)0733-9410(1991)117:1(89).

Yakhchalian, M., A. Nicknam and G. G. Amiri (2015). Optimal vector-valued intensity measure for seismic collapse assessment of structures, Earthq. Eng. Struct. Dyn., 14, 37-54, doi:10.1007/s11803-015-0005-6.

Yazgan, U. (2012). Proposal of energy spectra for earthquake resistant design based on turkish registers, Universidad Politécnica de Cataluña, Barcelona, 149.

Zapata-Franco, A. M., Y. F. Vargas-Alzate, J. M. Gonzalez and E. B. Olmos-Toledo (2025). FEM-based spectral matching to obtain specific surface spectra, Soil Dyn. Earthq. Eng., 190, 109153, doi:10.1016/j.soildyn.2024.109153.

Zapata-Franco, A. M., Y. F. Vargas-Alzate, L. G. Pujades and R. Gonzalez-Drigo (2023). Improved intensity measures considering soil inelastic properties via multi-regression analysis, Front. Earth. Sci., 11, doi:10.3389/feart.2023.1214536.

Zengin, E. and N. A. Abrahamson (2020). A vector-valued intensity measure for near-fault ground motions, Earthq. Eng. Struct. Dyn., 49, 716-734, doi:10.1002/eqe.3261.

Zhou, Y., P. Ge, J. Han and Z. Lu (2017). Vector-valued intensity measures for incremental dynamic analysis, Soil Dyn. Earthq. Eng., 100, 380-388, doi:10.1016/j.soildyn.2017.06.014.

Appendix A

Geotechnical properties of soil profiles.

ID	Material	Top (m)	Bottom (m)	Averg (m)	ρ (kg/m^3)	G_0	ɣ (gr/cm^3)	Vref (m/s)
1	Silty-Sand	0	6	3	1679.56	38.56	1.69	148.89
2	Silty-Clay	6	8.5	7.25	1706.40	35.00	1.62	142.80
3	Silty-Sand	8.5	12	10.25	1747.57	126.00	1.90	267.50
4	Silty-Clay	12	13.5	12.75	1793.67	119.67	1.60	258.00
5	Organic	13.5	14	13.75	1600.00	166.00	1.50	322.00
6	Silty-Sand	14	16	15	1719.25	165.75	1.83	305.50
7	Clay	16	17.5	16.75	1663.33	287.67	1.60	384.00
8	Organic	17.5	18	17.75	1800.00	97.00	1.40	232.00
9	Silty-Clay	18	22.5	20.25	1783.89	327.78	1.75	365.67
10	Organic	22.5	23	22.75	1800.00	119.00	1.40	257.00
11	Clay	23	29.5	26.25	1803.00	169.85	1.78	303.92
12	Organic	29.5	30	29.75	1800.00	683.00	1.40	616.00
13	Clay	30	35	32.5	1811.60	173.70	1.81	305.90
14	Clay	35	40.5	37.75	1797.50	194.40	1.80	323.70

Table A.1. Geotechnical properties – Profile 1.

ID	Material	Top (m)	Bottom (m)	Averg (m)	ρ (kg/m^3)	G_0	ɣ (gr/cm^3)	Vref (m/s)
1	Silty-Sand	0.00	4.50	2.25	1690.83	47.17	1.75	166.67
2	Organic	4.50	5.50	5.00	1685.50	47.00	1.47	167.00
3	Silty-Clay	5.50	7.00	6.25	1624.67	56.67	1.57	185.67
4	Organic	7.00	8.00	7.50	1789.00	64.50	1.62	189.50
5	Silty-Sand	8.00	13.00	10.50	1693.00	162.71	1.71	257.29
6	Clay	13.00	18.50	15.75	1710.18	62.82	1.65	191.45
7	Silty-Clay	18.50	21.00	19.75	1836.20	80.20	1.67	208.20
8	Clay	21.00	26.00	23.50	1746.20	100.90	1.68	239.70
9	Silty-Sand	26.00	29.50	27.75	1826.00	94.86	1.84	227.57
10	Clay	29.50	35.00	32.25	1811.09	119.18	1.69	255.82
11	Clay	35.00	40.00	37.50	1797.50	131.10	1.77	269.50

Table A.2. Geotechnical properties – Profile 2.

ID	Material	Top (m)	Bottom (m)	Averg (m)	ρ (kg/m^3)	G_0	ɣ (gr/cm^3)	Vref (m/s)
1	Silty-Sand	0.00	6.50	3.25	1679.00	83.90	1.77	206.20
2	Organic	6.50	7.00	6.75	1600.00	96.00	1.50	245.00
3	Silty-Clay	7.00	10.00	8.50	1708.83	79.00	1.74	211.50
4	Clay	10.00	11.50	10.75	1729.33	69.67	1.63	200.33
5	Silty-Clay	11.50	15.50	13.50	1740.75	93.75	1.73	231.63
6	Organic	15.50	16.00	15.75	1700.00	97.00	1.40	239.00
7	Silty-Clay	16.00	19.00	17.50	1763.33	108.83	1.72	247.33
8	Clay	19.00	26.00	22.50	1760.21	131.64	1.74	271.93
9	Clay	26.00	33.50	29.75	1826.21	156.36	1.80	290.93
10	Clay	33.50	40.50	37.00	1797.50	195.29	1.81	327.93

Table A.3. Geotechnical properties – Profile 3.

ID	Material	Top (m)	Bottom (m)	Averg (m)	ρ (kg/m^3)	G_0	ɣ (gr/cm^3)	Vref (m/s)
1	Silty-Sand	0.00	3.50	1.75	1780.00	67.20	1.78	192.40
2	Clay	3.50	6.00	4.75	1696.20	55.80	1.66	179.20
3	Silty-Clay	6.00	10.00	8.00	1785.71	94.86	1.79	226.29
4	Clay	10.00	11.50	10.75	1600.00	88.00	1.60	235.00
5	Organic	11.50	12.00	11.75	1500.00	89.00	1.50	244.00
6	Sand	12.00	13.00	12.50	1950.00	142.00	1.95	266.00
7	Silty-Clay	13.00	17.50	15.25	1800.00	123.33	1.80	260.56
8	Clay	17.50	25.00	21.25	1755.07	127.07	1.75	268.86
9	Clay	25.00	32.00	28.50	1782.14	158.79	1.79	296.57
10	Clay	32.00	40.50	36.25	1802.94	213.24	1.81	341.71

Table A.4. Geotechnical properties – Profile 4.

ID	Material	Top (m)	Bottom (m)	Averg (m)	ρ (kg/m^3)	G_0	ɣ (gr/cm^3)	Vref (m/s)
1	Silty-Sand	0.00	5.40	2.70	1815.14	934.29	1.81	511.57
2	Silty-Sand	5.40	8.90	7.15	1821.43	88.86	1.79	216.29
3	Silty-Clay	8.90	14.40	11.65	1754.55	99.55	1.72	236.45
4	Silty-Sand	14.40	16.90	15.65	1870.00	147.80	1.83	279.00
5	Clay	16.90	24.40	20.65	1758.80	175.87	1.71	305.00
6	Silty-Clay	24.40	26.90	25.65	1800.00	163.00	1.77	299.20
7	Clay	26.90	33.90	30.40	1771.43	191.00	1.74	322.64
8	Clay	33.90	40.40	37.15	1808.85	148.62	1.77	286.08

Table A.5. Geotechnical properties – Profile 5.

ID	Material	Top (m)	Bottom (m)	Averg (m)	ρ (kg/m^3)	G_0	ɣ (gr/cm^3)	Vref (m/s)
1	Organic	0.00	4.50	2.25	1620.00	686.80	1.56	509.40
2	Silty-Sand	4.50	7.50	6.00	1750.00	284.00	1.82	309.83
3	Organic	7.50	10.50	9.00	1516.67	341.83	1.50	355.33
4	Silty-Clay	10.50	15.50	13.00	1650.00	80.60	1.62	217.60
5	Silty-Sand	15.50	19.50	17.50	1843.75	139.88	1.87	274.63
6	Clay	19.50	26.00	22.75	1760.69	132.92	1.76	272.15
7	Clay	26.00	33.50	29.75	1803.85	175.15	1.79	309.69
8	Clay	33.50	40.00	36.75	1838.46	193.00	1.84	322.62

Table A.6. Geotechnical properties – Profile 6.

ID	Material	Top (m)	Bottom (m)	Averg (m)	ρ (kg/m^3)	G_0	ɣ (gr/cm^3)	Vref (m/s)
1	Organic	0.00	4.00	2.00	1600.00	154.00	1.57	269.00
2	Silty-Sand	4.00	6.50	5.25	1800.00	1167.00	1.77	558.80
3	Silty-Clay	6.50	8.00	7.25	1566.67	30.00	1.54	139.00
4	Organic	8.00	8.50	8.25	1600.00	35.00	1.57	148.00
5	Silty-Clay	8.50	9.50	9.00	1550.00	34.50	1.52	149.50
6	Clay	9.50	15.50	12.50	1641.67	57.00	1.61	184.75
7	Clay	15.50	22.50	19.00	1728.57	114.43	1.70	253.07
8	Clay	22.50	29.50	26.00	1735.71	154.14	1.71	294.43
9	Clay	29.50	40.00	34.75	1800.00	197.00	1.77	327.19

Table A.7. Geotechnical properties – Profile 7.

ID	Material	Top (m)	Bottom (m)	Averg (m)	ρ (kg/m^3)	G_0	ɣ (gr/cm^3)	Vref (m/s)
1	Silty-Clay	0.00	4.00	2.00	1775.00	38.75	1.74	146.75
2	Clay	4.00	5.50	4.75	1633.33	41.33	1.60	158.33
3	Organic	5.50	6.00	5.75	1400.00	60.00	1.37	207.00
4	Clay	6.00	7.00	6.50	1650.00	60.50	1.62	191.50
5	Silty-Clay	7.00	8.50	7.75	1800.00	78.33	1.77	208.00
6	Organic	8.50	9.00	8.75	1400.00	50.00	1.37	189.00
7	Clay	9.00	10.50	9.75	1800.00	90.67	1.77	224.67
8	Organic	10.50	11.00	10.75	1400.00	58.00	1.37	203.00
9	Silty-Clay	11.00	12.50	11.75	1800.00	232.00	1.77	331.67
10	Clay	12.50	16.50	14.50	1800.00	134.88	1.77	268.25
11	Clay	16.50	21.00	18.75	1772.22	128.67	1.74	266.67
12	Silty-Sand	21.00	23.00	22.00	1912.50	136.00	1.88	266.00
13	Clay	23.00	30.50	26.75	1833.33	145.07	1.80	280.07
14	Clay	30.50	40.00	35.25	1834.21	167.95	1.80	300.74

Table A.8. Geotechnical properties – Profile 8.

ID	Material	Top (m)	Bottom (m)	Averg (m)	ρ (kg/m^3)	G_0	ɣ (gr/cm^3)	Vref (m/s)
1	Silty-Sand	0.00	6.50	3.25	1770.00	65.20	1.74	188.70
2	Silty-Clay	6.50	14.00	10.25	1751.29	80.29	1.71	211.79
3	Silty-Clay	14.00	21.00	17.50	1792.86	104.07	1.76	240.50
4	Silty-Clay	21.00	28.00	24.50	1814.29	131.36	1.78	268.43
5	Silty-Clay	28.00	37.00	32.50	1838.89	170.94	1.81	303.72

Table A.9. Geotechnical properties – Profile 9.

ID	Material	Top (m)	Bottom (m)	Averg (m)	ρ (kg/m^3)	G_0	ɣ (gr/cm^3)	Vref (m/s)
1	Silty-Clay	0.00	17.00	8.50	1650.00	85.44	1.62	227.50
2	Silty-Sand	17.00	21.50	19.25	1844.44	104.46	1.81	237.78
3	Silty-Clay	21.50	31.50	26.50	1784.62	116.49	1.75	254.62
4	Clay	31.50	40.00	35.75	1791.18	129.65	1.77	268.71

Table A.10. Geotechnical properties – Profile 10.

ID	Material	Top (m)	Bottom (m)	Averg (m)	ρ (kg/m^3)	G_0	ɣ (gr/cm^3)	Vref (m/s)
1	Silty-Sand	0.00	12.20	6.10	1883.33	171.13	1.85	290.33
2	Silty-Clay	12.20	13.70	12.95	1700.00	83.33	1.67	221.33
3	Silty-Sand	13.70	18.20	15.95	1922.22	112.23	1.88	241.44
4	Silty-Sand	18.20	26.00	22.10	1898.18	278.22	1.84	317.55
5	Clay	26.00	34.00	30.00	1791.27	133.31	1.77	270.82
6	Clay	34.00	40.00	37.00	1845.27	133.14	1.81	268.55

Table A.11. Geotechnical properties – Profile 11.

***CORRESPONDING AUTHOR: Ana Maria ZAPATA-FRANCO**,
Universitat Politècnica de Catalunya, Department of Civil and Environmental Engineering, Jordi Girona 1-3, Barcelona, Spain
e-mail: ana.maria.zapata@upc.edu